1-1-2001

# Study of nanodynamics using the atomic force microscope

Rajeev Rajaram
*Iowa State University*

**Study of nanodynamics using the atomic force microscope**

by

Rajeev Rajaram

A thesis submitted to the graduate faculty

in partial fulfillment of the requirements for the degree of

MASTER OF SCIENCE

Major: Electrical Engineering

Major Professor: Murti V. Salapaka

Iowa State University

Ames, Iowa

2001

Graduate College
Iowa State University

This is to certify that the Master's thesis of

Rajeev Rajaram

has met the thesis requirements of Iowa State University

# TABLE OF CONTENTS

# LIST OF FIGURES

# LIST OF TABLES

# ABSTRACT

The Atomic Force Microscope (AFM) is a powerful tool for investigating surfaces at atomic scales. This thesis is a compilation of some interesting experiments that I performed on the AFM. The first experiment demonstrates the possibility of stochastic resonance, a unique phenomenon in which a deterministic and a stochastic signal cooperate to enhance the sensitivity of the AFM. Results indicate the presence of an optimal distance at which the AFM responds to weak sinusoidal signals better. The second experiment indicates that the AFM can also be used as an instrument to study and characterize piezoelectric properties of materials. The third experiment provides a method of measuring the spring constant of microcantilever.

# 1 EXPERIMENTAL STUDY OF STOCHASTIC RESONANCE IN ATOMIC FORCE MICROSCOPES

Stochastic resonance (SR) is an interesting phenomenon which can occur in bistable systems subject to periodic and random inputs. This phenomenon produces an improvement in the sensitivity of the bistable system to the periodic signal. The focus of this chapter is to see whether the Atomic Force Microscope (AFM), an instrument widely used to image samples with high resolution, exhibits stochastic resonance. The experimental results are presented which indicate that the AFM can be modeled as a bistable system in which stochastic resonance can be demonstrated. Stochastic Resonance if proved to be exhibited in the AFM, can be used to optimize the achievable resolution of imaging.

## 1.1 Introduction

It has been found that when signals comprising of noise and weak periodic components are fed into bistable systems like the Schmitt trigger, the system responds better to the periodic signal when the noise intensity is in a particular range ([1],[10]). The phenomenon of cooperation between a stochastic and a periodic signal is termed as stochastic resonance. The minimum amplitude of the periodic signal required to switch the system from one of its bistable states to the other is called the threshold. The periodic signal is termed weak if its amplitude is sub-threshold. The periodic signal has the effect of modulating the potential curve of the system as shown in Figure 1.1. The

system is depicted as a ball moving in a symmetric bistable potential having a potential barrier $\Delta V$. The potential is shown as being modulated when a sub-threshold periodic signal alone is fed to the system. In this case, the system oscillates about its present stable state and there is no transition into the other stable state. When the amplitude

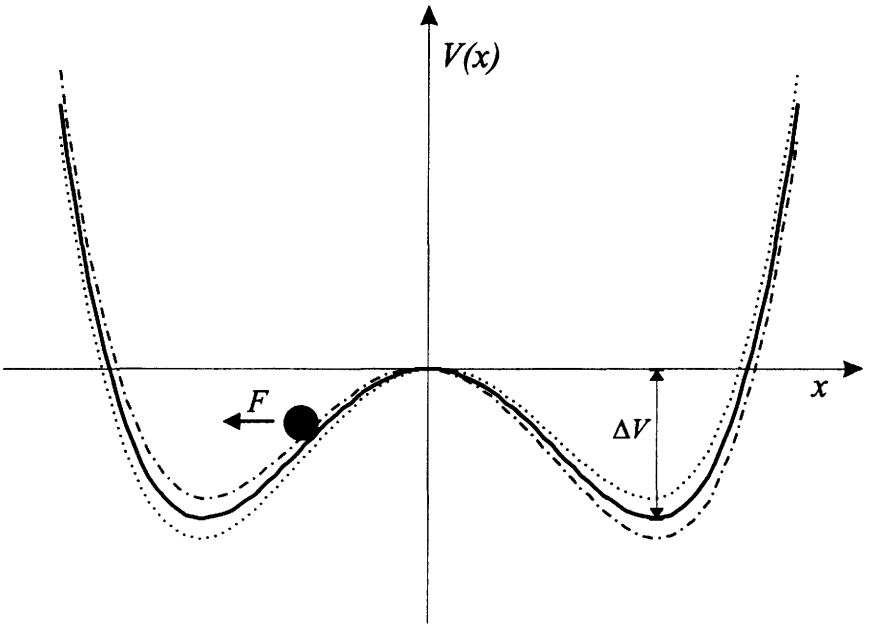


Figure 1.1 Sketch of a double-well potential function.

of the periodic signal is greater than the threshold, the system oscillates between the two states at a rate equal to the frequency of the periodic signal. When noise alone is fed into the bistable system, the system hops between its stable states at a probabilistic rate known as the Kramer's rate ([6]). When both signal and noise are fed together, at a particular noise intensity, the system begins to hop between its two states at the frequency of the periodic signal on an average. This is manifested as a peak in the output power spectral density (or equivalently the frequency spectrum) at the frequency of the deterministic signal. The plot of the output at the signal frequency as a function of the noise intensity displays a peak at the optimal noise intensity, indicating that optimal noise levels exist at which the system responds to the subthreshold periodic signal.

The method described above is the traditional way of observing stochastic resonance. Another way of investigating stochastic resonance is by changing the parameters of the system. This changes the bistable potential curve of the system and hence the potential barrier. This can make the existing noise intensity (which can be ambient thermal noise) optimal enough for the system to respond to the subthreshold signal.

In this chapter stochastic resonance is studied in the AFM by using the second method described above. The Schmitt Trigger, a bistable electronic circuit is also studied using the first method. Similarities in the behaviour of both systems are seen which leads to the strong belief that stochastic resonance can be used effectively in improving the resolution of the AFM.

In Section 1.2, a description of the AFM in its tapping mode of operation is given. The possibility of the AFM exhibiting stochastic resonance is investigated in Section 1.3. In Sections 1.4 and 1.5, the experiments done on the AFM and the Schmitt trigger are presented. The similarities in the response of both systems are discussed in Section 1.6 along with further improvements.

## 1.2 Introduction to the Atomic Force Microscope

The Atomic Force Microscope has revolutionized high resolution imaging of samples. A schematic of the AFM is shown in Figure 1.2. The tapping mode operation of the AFM has been widely used to image samples. In this mode, the cantilever is made to tap the sample surface as it scans the sample. The cantilever is mounted on a dither piezoelectric drive. The dither piezo is subjected to a sinusoidal forcing at the resonant frequency of the cantilever. The sample is positioned using a high voltage piezoelectric scanner which can move in all three directions in space. Due to the force of interaction between the cantilever and the sample, the amplitude of the first harmonic of the oscillation changes. The sample can be positioned by applying voltages in the Z direction to control the

movement. A LASER beam is focused on the tip of the microcantilever. The reflected beam is detected using a photodiode detector cell, which converts the movement of the cantilever into an equivalent change in voltage. This detection system provides a large optical lever and hence minute variations in the cantilever's displacement are amplified as a large voltage signal. The piezo scanner tube is subjected to a raster scan motion in addition to a feedback control action in the Z-direction. The control law tries to maintain a constant amplitude of oscillation by moving the sample in the Z-direction. The Z-movement is recorded along with the X-Y scan information and an image of the sample profile is obtained by mapping this information with appropriate color codes. The AFM has been successfully used to image samples with resolutions of the order of 1 Angstrom.

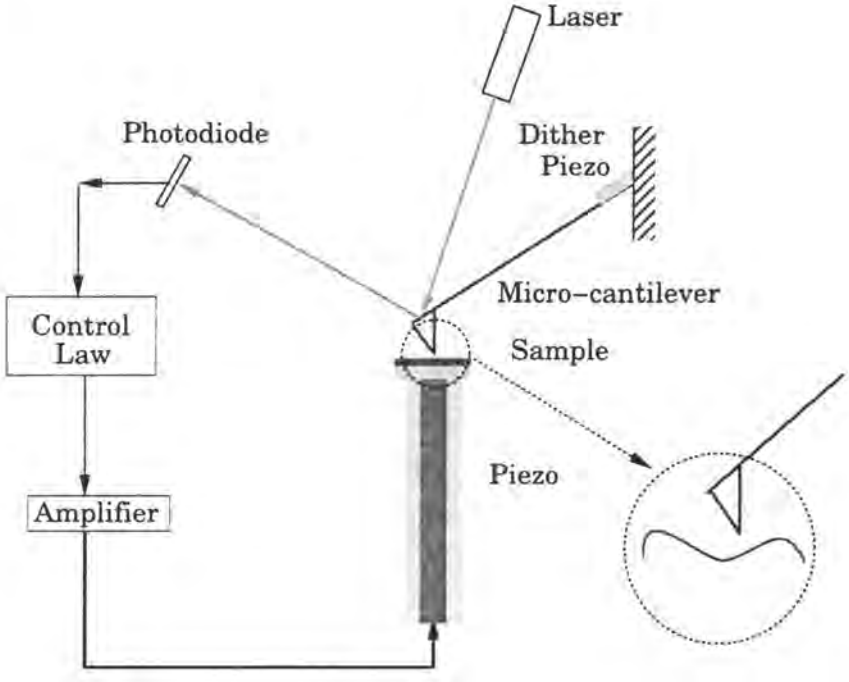


Figure 1.2 A schematic of the AFM

## 1.3 Stochastic Resonance in the AFM

In the context of stochastic resonance, the AFM can be modeled using an asymmetric bistable potential curve. The equation of the potential curve of the AFM when the cantilever is inside the sample potential is given by

$$V(p) = \frac{k}{2}p^2 - \frac{d}{(p+Z)} + \frac{\Sigma^6 d}{210(p+Z)^7} + \theta. \tag{1.1}$$

where, $k$ is the spring constant of the cantilever per unit mass, $Z$ characterizes distance between the cantilever and the sample, $\Sigma$ and $d$ are parameters that depend on the nature of the sample and the cantilever, $p$ is the position of the tip of the cantilever measured from the local maximum of the double well potential curve and $\theta$ is a constant chosen to make the position of maximum as zero([2],[3]). Equation 1.1 is the sum of the potential energy of the cantilever and the potential curve describing the interatomic force of interaction between the cantilever and the sample, and hence describes only the conservative forces that act on the system. The potential function is plotted in Figure 1.3, which is clearly an asymmetric bistable potential curve. The two wells are distributed asymmetrically about the potential maximum, as compared to Figure 1.1. This potential curve is seen to be a function of the cantilever spring constant $k$ and the distance of separation between the cantilever and the sample $Z$. This is seen in Figures 1.4 and 1.5. It is evident from these figures that a change in $k$ or $Z$ changes the potential barrier $\Delta$V, which might favor a transition of the cantilever from one well to the other. The dependence on $Z$ can be of significant importance for example, in increasing the sensitivity of the AFM by varying $Z$ which, in turn changes the potential curve.

The AFM when subjected to both noise and a periodic signal can be described as the following stochastic process:

$$\begin{cases} \dot{p} = v \\ \dot{v} = -V'(p) - \eta v + \sigma\,\xi(t) + \epsilon\cos\omega_0 t \end{cases} \tag{1.2}$$

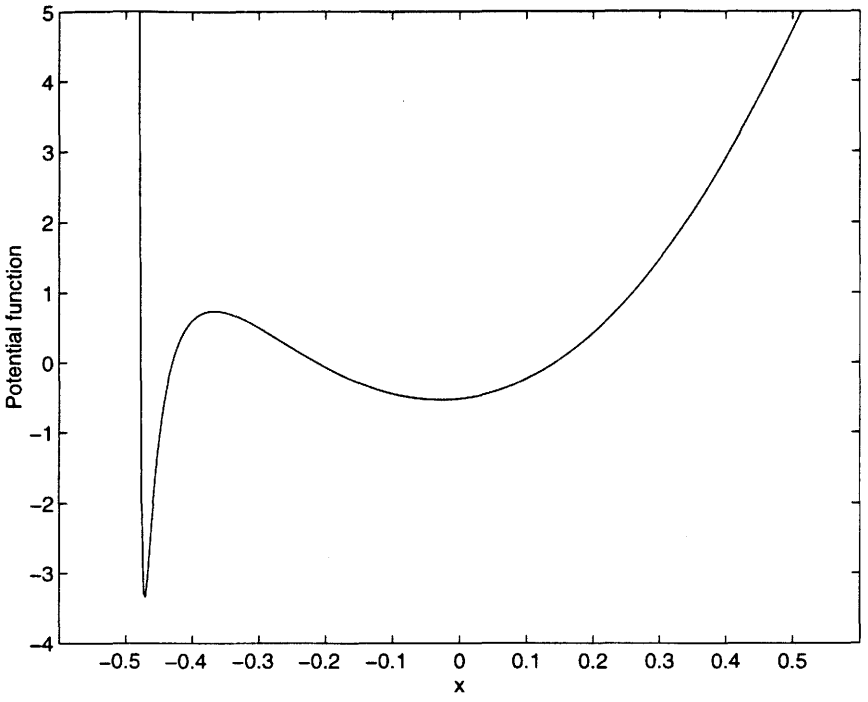


Figure 1.3 Bistable potential curve of the AFM

where the random variables $p$ and $v$ denote position and velocity of the cantilever having unitary mass, $V(p)$ is the potential function, $\eta$ is the damping factor, $\sigma\,\xi(t)$ is a white noise with variance $\sigma^2$ and $\epsilon$ is the amplitude of a sinusoidal modulation of the force. The noise is the thermal noise which is present in the AFM. When subjected to noise alone, the transition rate between the two states is equal to the Kramer's rate ([9]). In [3], systems having asymmetric potential curves are shown to exhibit stochastic resonance, the assumption being that the continuous state system can be approximated as a discrete state system consisting only of the two stable states. This approximation holds under the assumption that the sinusoidal input signal has a period which is large with respect to the *relaxation time*, defined as the time for probability to equilibrate within one well. The discrete state system is modeled by the following rate equation

$$\frac{dn_R}{dt} = -\frac{dn_L}{dt} = W_L(t)n_L - W_R(t)n_R \tag{1.3}$$

where $n_L$ and $n_R$ are the probabilities of finding the system in the left and right potential

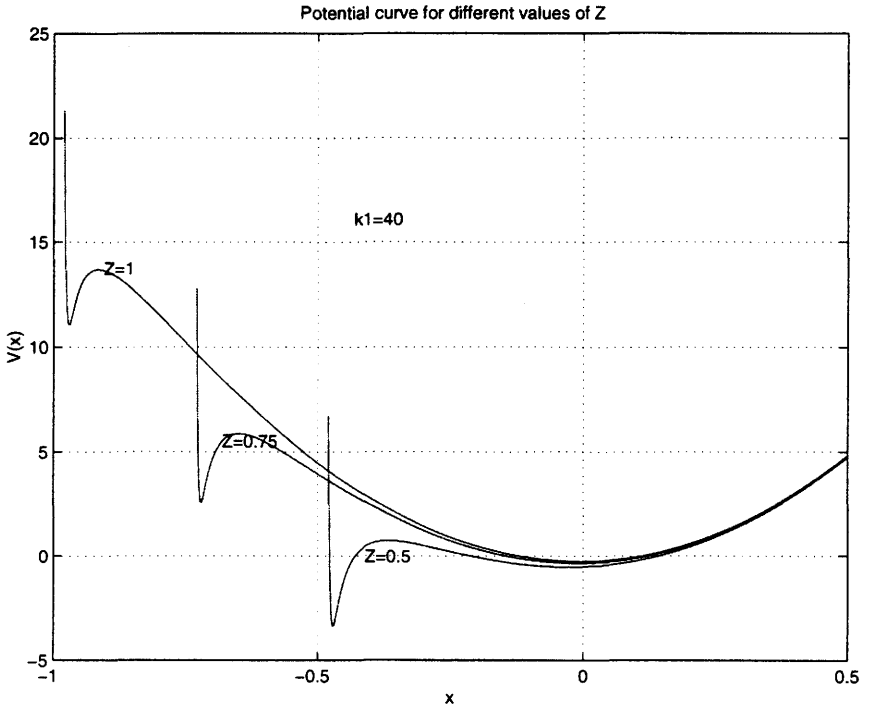


Figure 1.4 Dependence of the double well potential function on the cantilever sample separation

wells respectively, and $W_L$ and $W_R$ are the rate of transitions from the left and right wells respectively.

In what follows, experiments performed on the AFM and the Schmitt trigger to study stochastic resonance are presented.

## 1.4 Experiments to Observe Stochastic Resonance on the AFM

In this section, experiments are presented which demonstrate stochastic resonance in AFM. The entire section is motivated by the experimental observation of the AFM's sensitivity to a 100mV, 1kHz(the cantilever's resonant frequency was 298.38kHz) sinusoidal forcing signal. In section 1.4.1 the cantilever's frequency response is characterized and the quality factor is found out experimentally. Sections 1.4.2 and 1.4.3 describe experiments to obtain the sensitivities of the photodiode detector and the dither piezo

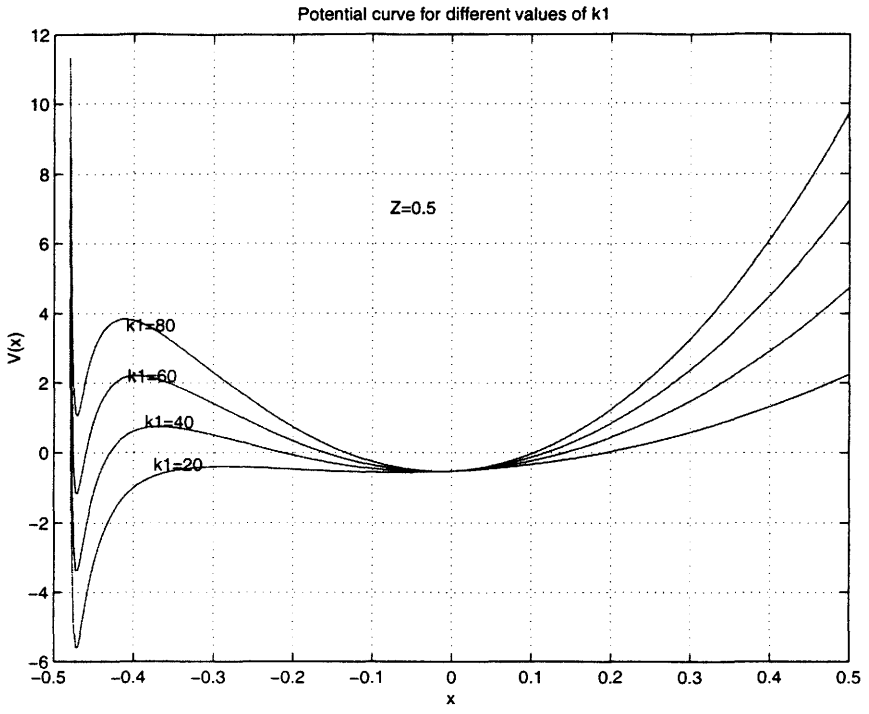


Figure 1.5 Dependence of the double well potential function on the cantilever spring constant

which holds the microcantilever. These are required to confirm that the forcing signal is indeed subthreshold. In section 1.4.4, the potential curve of the AFM is obtained experimentally at the cantilever-sample separation where the AFM showed improved sensitivity. In section 1.4.5, the threshold voltage required to just make the cantilever hop between the two wells is determined. Section 1.4.6 connects all the previous sections and concludes the experiment on the AFM confirming the fact that stochastic resonance happens in the AFM. In what follows, a minimum level of operational knowledge of the AFM is assumed.

### 1.4.1 Experiment to determine the frequency response of the tapping mode cantilever

The frequency response of the chosen tapping mode cantilever was determined experimentally by recording the photodiode's readout for sinusoidal voltages having an amplitude of 50mV and frequency ranging from 296.5 to 300.5 kHz. The magnitude plot is as shown in Figure 1.6. The IN0 pin of the Signal Access Module (SAM) was used to provide the sinusoidal forcing signals to the cantilever.

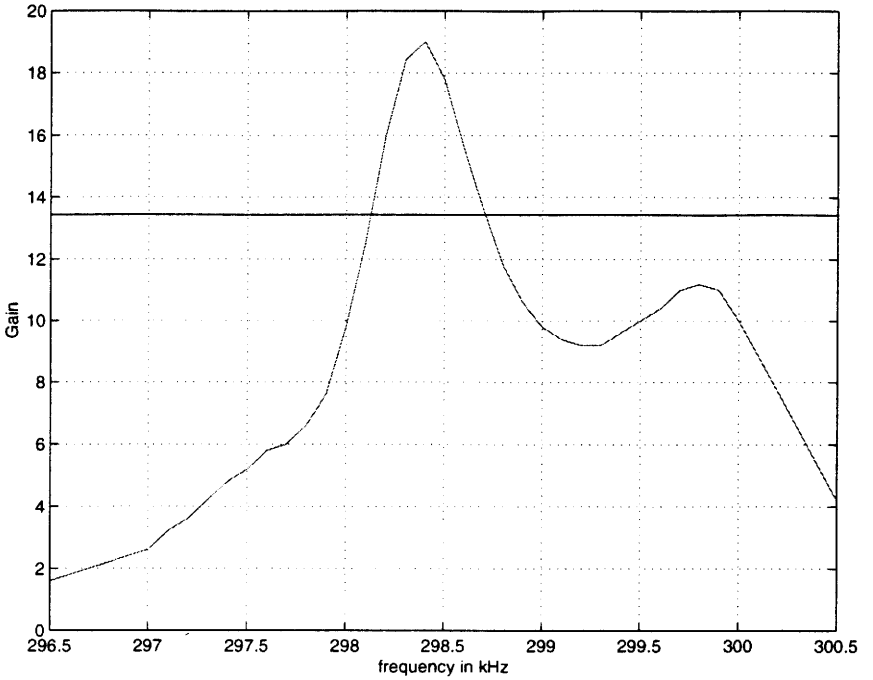


Figure 1.6 Experimentally observed gain of the cantilever as a function of input sinusoidal frequency

The half power points are joined by a line and the quality factor was found out from the point of intersection of this line with the frequency response curve using Equation 1.4. The cantilever is usually modelled as a second order system near its resonant frequency ([8])(although it might have more than a single mode of resonance at other frequencies) which has the standard second order resonance curve as its frequency response. There are two half power points on either side of the resonance peak, and the quality factor is

calculated as given in Equation 1.4. This fact is evident in the experimentally observed frequency response in Figure 1.6.

$$Q = \frac{f_0}{\triangle f} \tag{1.4}$$

where $f_0$ is the resonant frequency in kHz and $\triangle f$ is the difference between the half power frequencies(otherwise known as the bandwidth). The Q factor was found experimentally to be 510. The spring constant of the cantilever is typically determined using thermal noise response analysis. The spring constant was taken to be 20N/m which is a typical value for tapping mode cantilevers.

### 1.4.2 Determination of photodiode sensitivity

The experimental data for cantilever movement was obtained in volts, hence the photodiode had to calibrated to convert this into position units($nm$). The calibration of the photodiode detection system is typically done from a force curve experiment. The force curve is a plot of the amplitude of oscillation as a function of the distance of separation between the cantilever and the sample. In order to obtain a force curve, the AFM is switched from the normal imaging mode to what is known as the Force Calibration mode. In this mode, the control action is stopped and instead the sample is moved in a ramp fashion to and from the cantilever, which is still oscillating at resonance. The amplitude of oscillation is captured and plotted as a function of the distance of separation between the cantilever and the sample. The force curve is in essence a characteristic of the sample itself and could be used to obtain sample parameters [8]. The slope of the force curve (for hard samples) will directly give the sensitivity of the photodiode detection system in V/nm.

The AFM is equipped with software which can be used efficiently to obtain a force curve. The slope can be found out by just using the mouse to draw a line parallel to the force curve. A force calibration plot was obtained for the mica sample using the AFM

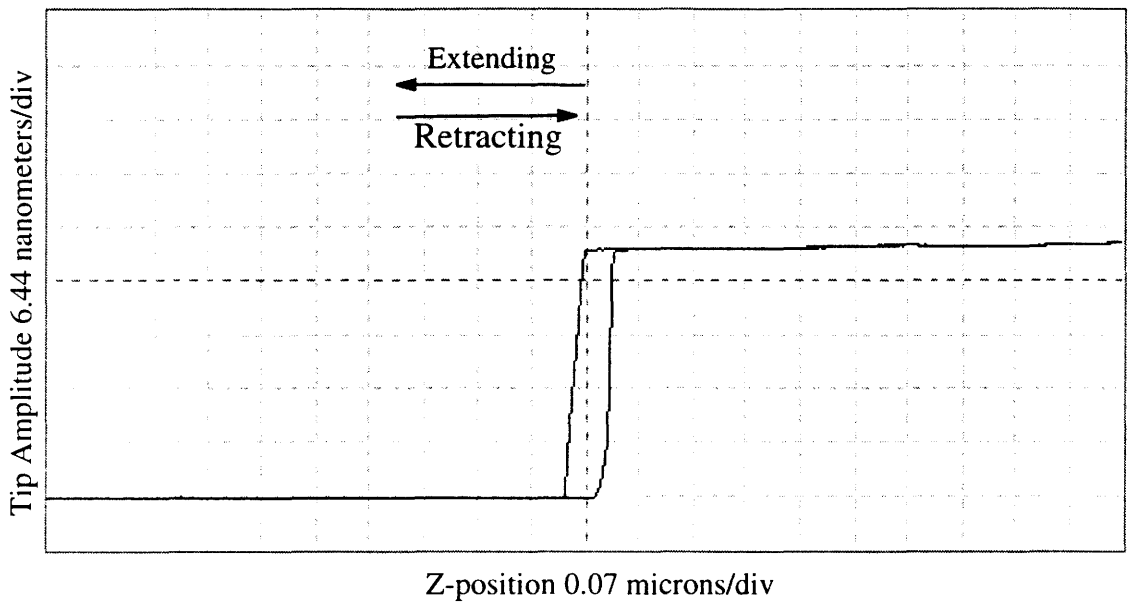


Figure 1.7 Force Calibration plot for the mica sample

and it is shown in Figure 1.7. The sensitivity from the force curve was determined to be 0.0766V/nm.

### 1.4.3 Determination of the dither piezo sensitivity

The cantilever can be viewed as an interconnection of two systems, namely the dither piezo which is used to oscillate the cantilever and the cantilever itself (Figure 1.8).

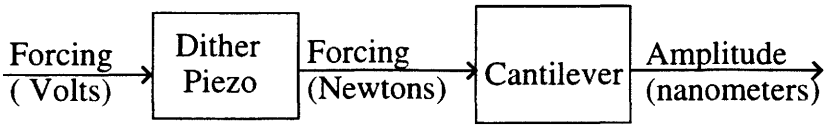


Figure 1.8 The cantilever viewed as an interconnection of two systems

The dither piezo can be viewed as a transducer which converts voltage inputs to force. The sensitivity of the dither piezo can be assumed to be a constant throughout the frequency range of operation of the AFM. The commercial AFM comes equipped with a breakup box called the Signal Access Module (SAM), which can be used to monitor and input signals to the various electronic modules of the AFM. However, the SAM can be used only to force the dither piezo (using voltage inputs) and measure the cantilever's movement. The equivalent forcing (in Newtons) that the dither piezo provides to the cantilever is unknown and hence it has to be determined indirectly by the procedure described below.

The following equations describe the relationship between the cantilever's oscillation amplitude (in meters) at resonance and the forcing (in Newtons).

$$\epsilon = \frac{kA_{res}}{Q} \tag{1.5}$$

where $\epsilon$ is the forcing amplitude in *Newtons*, $A_{res}$ is the cantilever's amplitude at resonance in *meters*, $k$ is the spring constant of the cantilever and $Q$ is the quality factor of the cantilever. In Equation 1.5 the quality factor determined in Section 1.6 can be

used. In order to determine the sensitivity of the dither piezo, the dither piezo was forced for different voltage values and the amplitude of oscillation was read out from the AFM directly. Table 1.1 shows the experimentally obtained data, where $D_i$ is the dither input in millivolts and $C_o$ is the cantilever's output as measured by the photodiodes. The photodiode sensitivity (Section 1.4.2) was used to convert the photodiode output into nanometer units. Then Equation 1.5 was used to calculate the dither piezo's output in Newtons. This was tabulated for different voltage inputs and the sensitivity was obtained using Equation 1.6.

Table 1.1 Tabulated experimental data for determining the sensitivity of the dither piezo

| S.No | $D_i(mV)$ | $C_o(Vrms)$ | $S_d(nN/V)$ |
|---|---|---|---|
| (1) | 50 | 0.9500 | 0.0980 |
| (2) | 60 | 1.1200 | 0.0963 |
| (3) | 70 | 1.2800 | 0.0944 |
| (4) | 80 | 1.4700 | 0.0948 |
| (5) | 90 | 1.6200 | 0.0929 |
| (6) | 100 | 1.7800 | 0.0918 |
| (7) | 110 | 1.9500 | 0.0915 |
| (8) | 120 | 2.1200 | 0.0912 |
| (9) | 130 | 2.3000 | 0.0913 |
| (10) | 140 | 2.6100 | 0.0962 |
| (11) | 150 | 2.7800 | 0.0956 |

$$S_d = \frac{\epsilon}{V_{input}} \tag{1.6}$$

where $S_d$ is the sensitivity of the dither piezo, $\epsilon$ is the forcing amplitude in Newtons and $V_{input}$ is the input to the dither piezo in Volts. The sensitivity was tabulated and an average was obtained to be $S_d$=0.0940 nanonewtons per volt.

Using this sensitivity, the threshold in Newtons obtained in Section 1.4.5 can be converted to volts. This was found to be 2.1277V. The last thing that remains to be checked is whether the AFM is sensitive to an input that is less than 2.1277V.

### 1.4.4 Experiment to obtain the potential curve of the AFM

The potential curve of the AFM was theoretically shown to be an asymmetric double well curve. The Boltzmann law says that if a system is in thermal equilibrium with the environment and is described by a potential function $V(p)$, where $p$ is the position, then the probability of finding the system at position $p$ is proportional to $exp(-V(p))/k_bT$ where $k_b$ is the Boltzmann's constant and $T$ is the temperature in Kelvin units i.e

$$P(p) = C' \exp(\frac{-V(p)}{k_bT}) \tag{1.7}$$

where $P(p)$ is the probability of finding the system in position $p$ and $C'$ is a proportionality constant. Taking natural logarithms on both sides of 1.7 we get

$$V(p) = C - \ln(P(p))k_bT \tag{1.8}$$

where $C = \ln(C')$.

In this experiment, the AFM was operated in the tapping mode. The AFM was false engaged and changed into the Force Calibration Mode. In the Force Calibration mode of the AFM, the Z piezo (the sample holder) can be moved near the cantilever by changing the Z-Scanstart parameter keeping the Zscansize parameter as zero. The cantilever was introduced into the sample potential with the input being ambient thermal noise. The objective of this experiment was to obtain the potential curve of the AFM at a particular cantilever-sample separation($Z$). The photodiode output was captured from the IN0 pin of the Signal Access Module(SAM, used to access the signals in and out of the AFM) using a DSP card(M44) which has data acquisition capabilities. The obtained data was then histogrammed for 30 voltage bins. The histogram data contained the number of points that occurred at the different photodiode output voltage (or equivalently position) bins. If $N_1$ is the number of data points that occurred at a particular position bin, and $N$ is the length of the data, the probability of finding the cantilever in that position is

given by

$$P(p) = \lim_{N \to \infty} \frac{N_1}{N} \tag{1.9}$$

The negative natural logarithm of the histogrammed data was plotted as a function of the 30 position bins. The position bins were in equivalent voltage units as measured by the photodiode cells. The experimental result is as shown in Figure 1.9 for a given cantilever-sample separation $Z$.

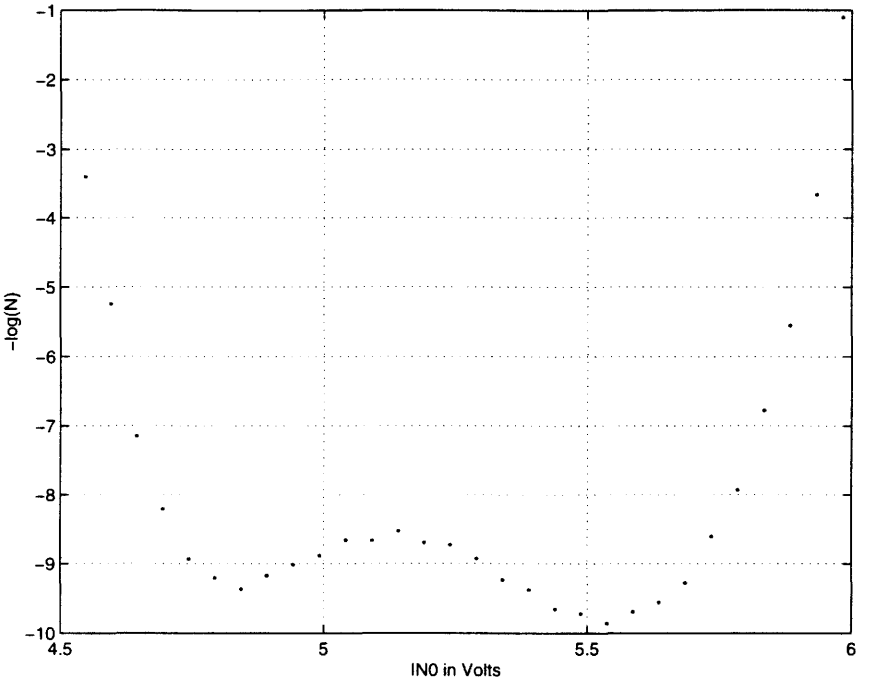


Figure 1.9 Experimentally observed potential curve of the AFM for a given cantilever-sample separation

It is clear from the experimental curves that the potential is double welled and asymmetric. This is in practice a difficult experiment to carry out as the piezo starts to drift and it is difficult to maintain the cantilever at a fixed distance from the sample. The more the number of data, the better is the approximation to the probability in Equation 1.9. However, waiting for a long time to acquire data would cause the piezo's drift to affect the potential curve by changing the parameter $Z$ in Equation 1.1 thereby

changing the potential curve itself. Hence the objective of the experiment was a little difficult to be met.

### 1.4.5 Determination of threshold voltage

The first thing to be done in order to observe stochastic resonance in the AFM is to determine the threshold forcing which will just make the AFM to hop between the two wells. The double well potential curve was obtained in the previous section within a proportionality constant. It is difficult to experimentally obtain the threshold forcing,hence simulations were performed to obtain the forcing amplitude in force units (*Newtons*). The experimentally obtained potential curve data was loaded into MATLAB. The x-axis was normalized in order to make the local maximum occur at 0 position. The value of the forcing amplitude $\epsilon$ (in *Newtons*) was changed in the simulation until the modulated potential curve looked as though the wells are about to dissappear, which would mean that the AFM will be made to hop between the wells for any $\epsilon$ greater this value. Figure 1.10 shows the simulation result.

It is clear from Figure 1.10 that for $\epsilon$=2e-10 *Newtons* or higher, the cantilever will surely hop between the two wells and also that any forcing less than 2e-10 Newtons will not be sufficient for the cantilever to cross the barrier and hop between the wells . Hence the threshold forcing amplitude was determined to be 2e-10 Newtons. The next experimental step was to observe if the AFM is sensitive to a forcing less than 2e-10 Newtons. Using the dither piezo sensitivity, the threshold in Newtons can be converted to volts. This was found to be 2.1277V. The last thing that remains to be checked is whether the AFM is sensitive to an input that is less than 2.1277V.

### 1.4.6 Stochastic resonance

A cantilever having a resonant frequency of 298.38 KHz was chosen for the experiment. A mica sample was cut into a square size of half an inch side, and the surface was

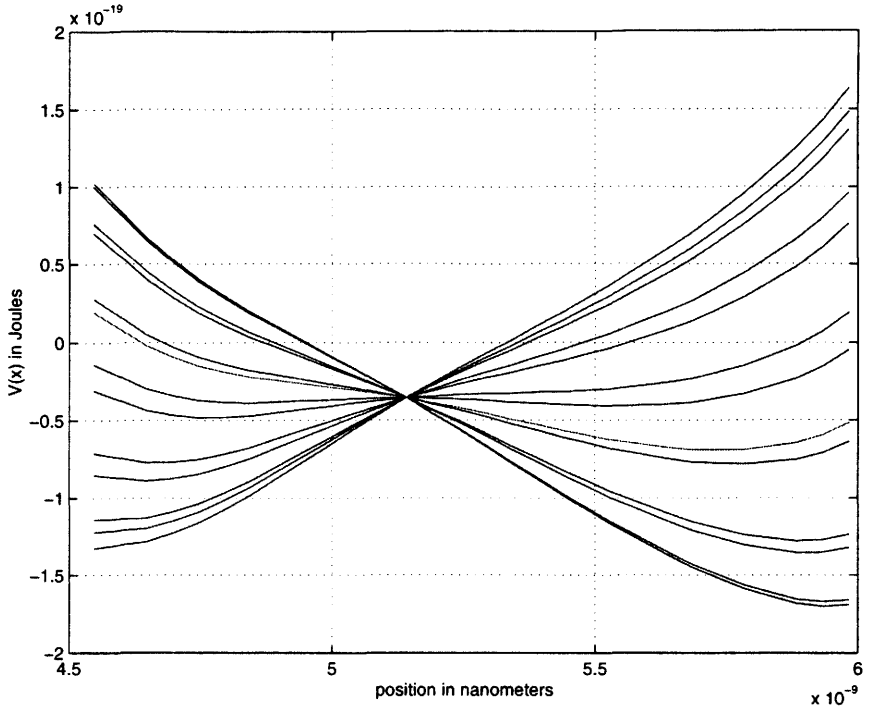


Figure 1.10 The modulated potential curve for $\epsilon = 2e - 10$

scraped using a gum tape to obtain a new layer. The sample was carefully mounted on to the sample holder (Figure 1.2). The cantilever was initially subjected to a 100mV 1 KHz sinusoidal voltage when outside the sample potential. The amplitude (100mV) was chosen to be lesser than the threshold value as calculated in the previous section(2.1227V). The sinusoidal voltage was generated using a HP-33120 signal generator. The FFT of the cantilever's response did not show any significant component at 1 KHz (see Figure 1.11).

The response was predominantly noisy as seen in Figure 1.11. This was as expected because the frequency (1 KHz) was far away from the resonant frequency of the cantilever (298.38 KHz). The cantilever was then introduced into the sample potential in steps of 50 nanometers. This was done by first exciting the cantilever at resonance and then introducing it into the sample potential till the oscillation amplitude of the cantilever started reducing. The same 100 millivolt 1 KHz signal was fed into the cantilever. It was

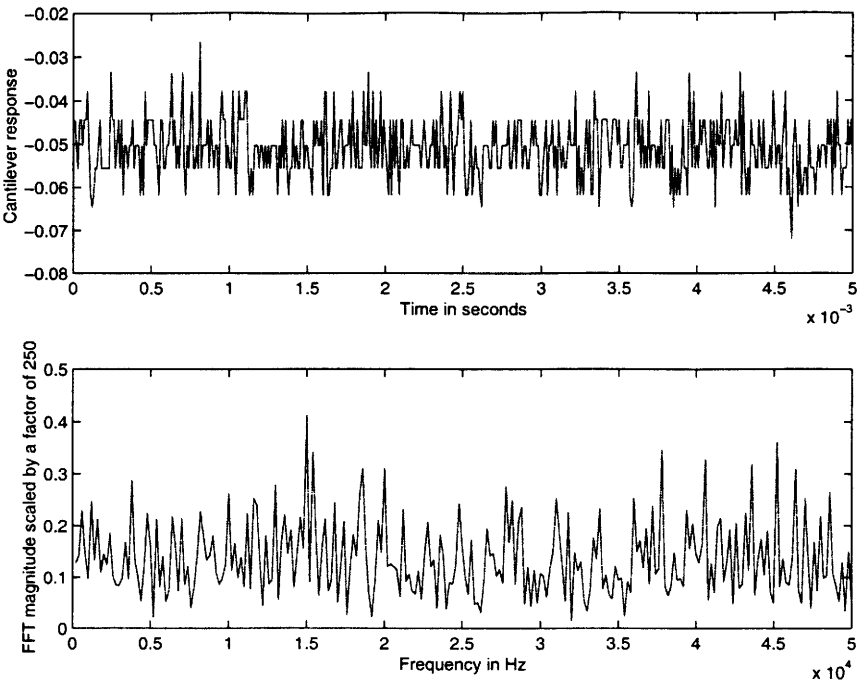


Figure 1.11 Experimental results on the AFM when cantilever is outside the sample potential

found that the cantilever, whose response was adversely affected by noise when outside the sample potential, started responding to the same when inside sample potential. The response and the frequency spectrum of the cantilever when inside and outside the sample potential are shown in Figures 1.11 and 1.12. The output was seen to be a noisy 1 KHz sine wave when the cantilever was kept inside the sample potential. A change in the frequency of the input resulted in a change in the frequency of the FFT peak of the cantilever's response when inside the sample potential. It was found that the FFT peak at 1kHz was a function of the cantilever sample distance and the dependence is as shown in Figure 1.13. It is evident from the figure that there exists an optimal distance of separation between the cantilever at which the cantilever responds better to the sinusoidal signal.

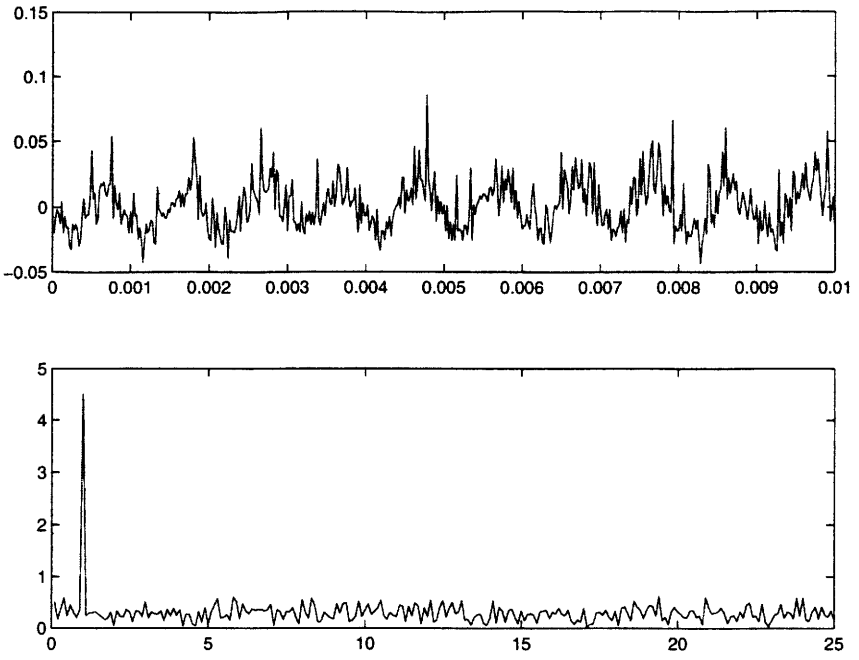


Figure 1.12 Experimental results on the AFM when cantilever is inside the sample potential

## 1.5 Schmitt Trigger

### 1.5.1 System description

The Schmitt trigger is an electronic circuit which has two stable states. This is a positive feedback circuit which compares the input voltage to a fixed threshold. A schematic of the Schmitt trigger is shown in Figure 1.14. The output goes high if the input is higher than the threshold and vice versa. The high and low states of the Schmitt trigger are the two saturation states of the amplifier ($V_{sat} = \pm 12$ Volts). ECG778A high bandwidth (50 MHz) amplifier was used to build the circuit. As shown in Figure 1.14, the threshold is chosen by fixing the values of the resistors $R_1$ and $R_2$ and is given by $V_t = R_1/(R_1+R_2)|V_{sat}|$. When a sinusoidal signal is fed as input, the output is a square wave of same frequency if the amplitude of the input is greater than the threshold. The Schmitt trigger can be in one of its two stable states when no input is fed into it. In

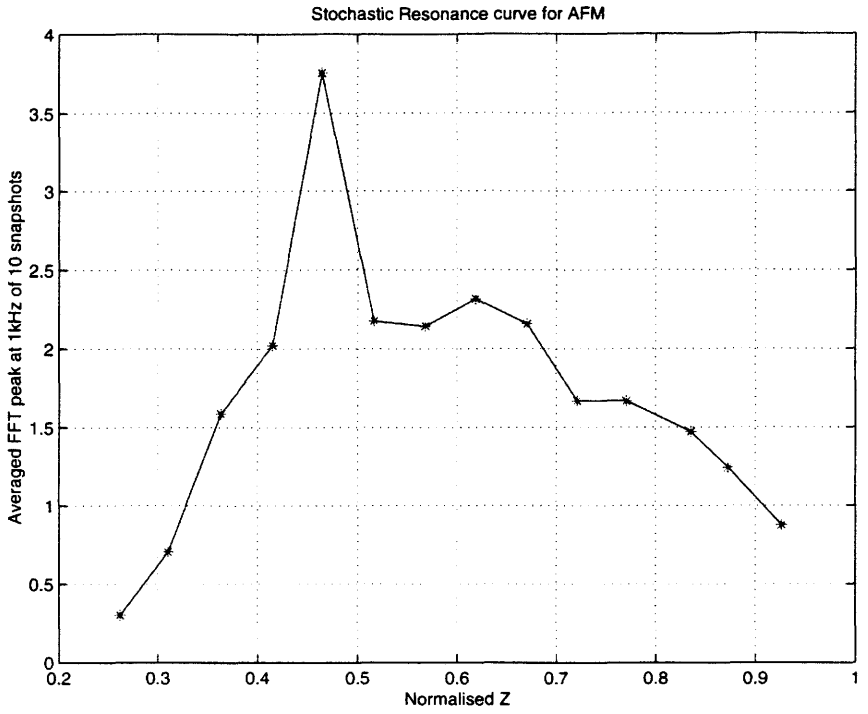


Figure 1.13 Stochastic Resonance in AFM

the following section the results of experiments on the Schmitt trigger circuit which demonstrate stochastic resonance are presented.

### 1.5.2 Experimental results

The value of the threshold was fixed at 2 Volts by choosing $R_1$ to be 2 KΩ and $R_2$ to be 10 KΩ. A sinusoidal voltage of 1 Volt amplitude and 1 KHz frequency was fed as input. The circuit remained in one of its stable states and no switching was observed as expected. Band-limited white noise was added to the input and the intensity of the noise was varied from 1 Volt to 9 Volts. The signal output at 1 KHz attained a maximum for a noise intensity of approximately 3 Volts as shown in Figure 1.16. The noise was confirmed to be band limited and white by verifying that its Fast Fourier Transform (FFT) was a flat band till a frequency of 60 MHz. A HP-33120 signal generator was used to generate the two inputs. The FFT's were generated using HP-VEE (Visual

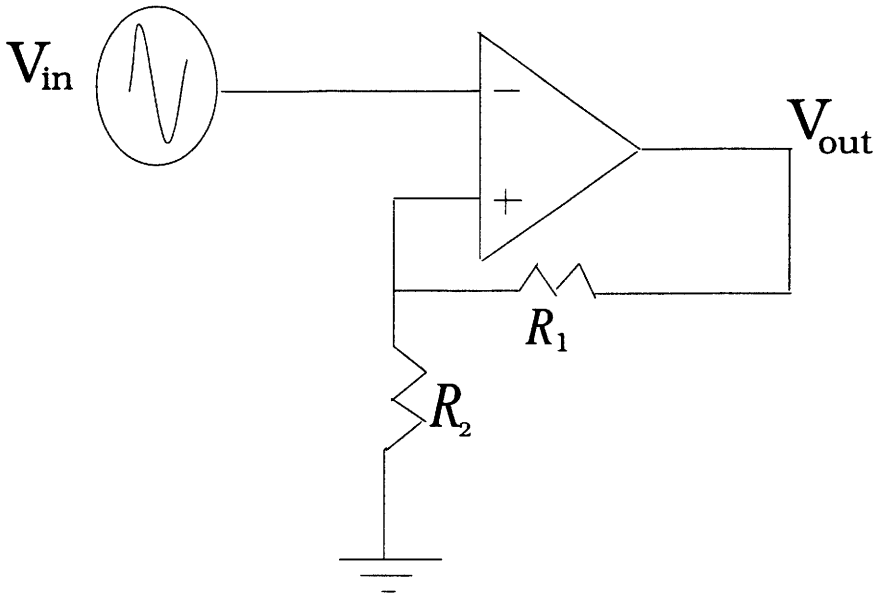


Figure 1.14 Schematic of a Schmitt Trigger.

Engineering Environment) software. The FFT of the output was averaged 100 times for noise intensities varying from 1 Volt to 9 Volts. The output signal was a square wave at 1 KHz superimposed with noise (see Figure 1.15). Here again a change in frequency of the sinusoidal input resulted in an equal change in the frequency of the FFT peak.

## 1.6 Discussion and further improvements

The effect of adding a weak periodic signal to the Schmitt trigger and the AFM look similar as shown in Figures 1.12 and 1.15. When noise and a weak sinusoidal signal are fed together, the Schmitt trigger shows switching between its bistable states which, on an average resembles the switching due to the pure sinusoidal signal alone. This is confirmed by the FFT of the Schmitt trigger's response in Figure 1.15. Similar to this, the cantilever of the AFM when inside the sample potential attains two states as shown in the cantilever response in Figure 1.12. Also the cantilever whose response is corrupted by noise when outside the sample potential (Figure 1.11) starts showing a peak in its FFT at the frequency of the sinusoidal input, when inside the sample potential. The

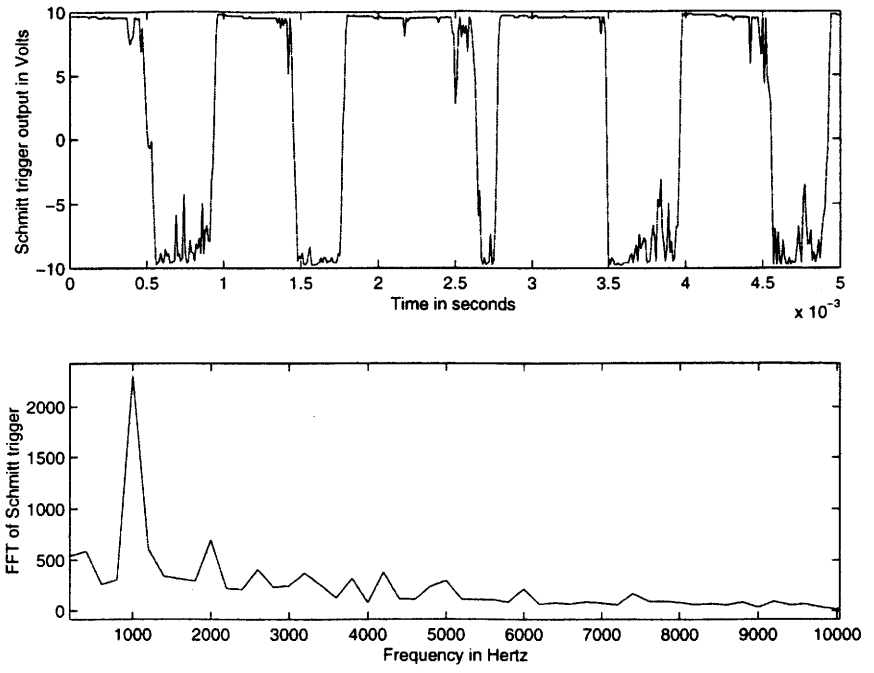


Figure 1.15 Experimental results on the Schmitt trigger

two states attained by the cantilever are suspected to be the free state and being stuck to the sample, respectively. A change in the frequency of the sinusoidal input shifted the output FFT peak frequency in both systems. Introducing external noise into the Schmitt trigger improved the deterministic component in the output as shown in Figure 1.16, which clearly shows a maximum attained by the FFT peak at signal frequency. Similarly a change in the $Z$ parameter in the AFM improved the sensitivity of the cantilever at a certain value of $Z$. This leads to the strong belief that the thermal noise present inside the AFM is enough for stochastic resonance to occur.

More experiments conducted on the AFM at lower ambient temperatures and reduced levels of sinusoidal voltage can determine the levels of thermal noise inside the AFM at which the increased sensitivity of the AFM to the weak periodic signal can be attained. Position feedback can be used to vary the effective spring constant $k$, of the system. The dynamics would then look like

$$m\ddot{p} + c\dot{p} + (k + k_1)p = F(t) + kb(t) \tag{1.10}$$

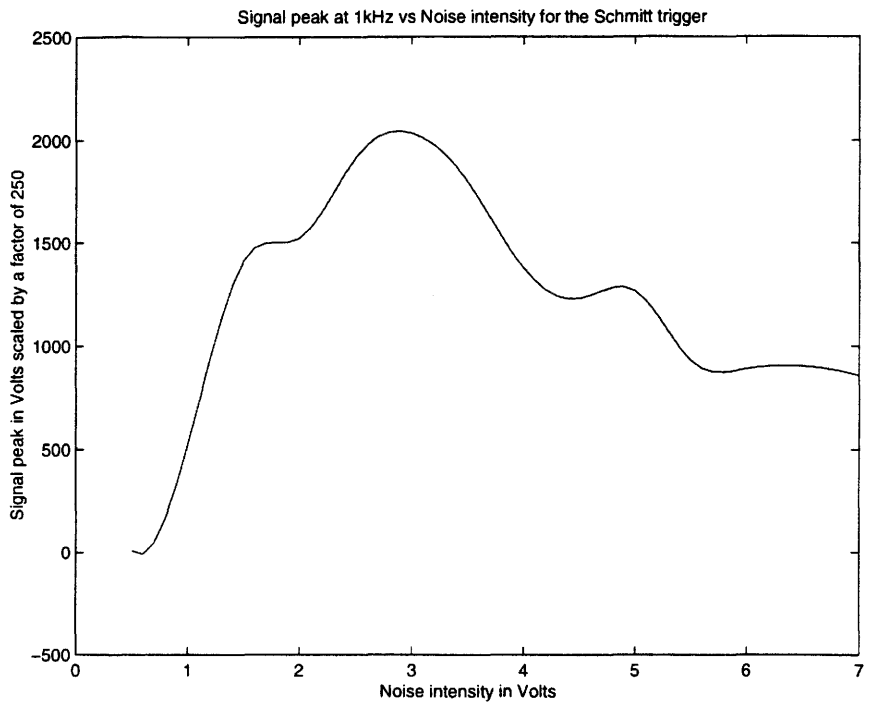


Figure 1.16 Signal peak vs Noise intensity exhibiting a maximum

where $k_1$ is the change in the original spring constant $k$ of the cantilever due to position feedback. As seen in Equation (1.1) and Figure 1.5, a change in the spring constant effectively changes the shape of the potential curve, and a change in the potential curve would in turn change the threshold value and could make the ambient thermal noise level optimum enough to produce maximum sensitivity of the AFM to a weak periodic signal. The cantilever can thus be made to respond better to weak periodic signals by varying the effective spring constant using position feedback. The spring constant when varied can make the inherent thermal noise optimum for stochastic resonance to happen. This would mean that for that value of $k_1$ which is externally set for the controller, the AFM has maximum sensitivity to a weak periodic signal. Hence the sensitivity of the AFM can be optimized by using position feedback. In [3], an expression of the signal to noise ratio has been derived. Further research needs to be done in verifying and understanding the sensitivity of that expression to system parameters.

Equation (1.1) describes how the potential curve of the AFM varies with the cantilever spring constant $k$ and the cantilever sample separation $Z$. The expression $-V'(p)$ (the negative derivative of the potential function) directly gives us the net force acting on the cantilever, where $V(p)$ is the total potential energy of the cantilever and the sample interaction as a function of $p$, the displacement of the cantilever. The parameters $\Sigma$ and $d$ in Equation (1.1), depend on the cantilever and sample properties. This means that different samples will exhibit different potential curves, which in turn will mean that the effect of stochastic resonance on the cantilever output will be different for different samples. This can be used to characterize different samples which is a topic of future research. The fact that the AFM responds in a manner similar to the Schmitt trigger when subjected to sinusoidal and noise inputs (the noise input to the AFM being assumed to be thermal noise) makes it more evident that the AFM can be modeled as a discrete state system in certain range of cantilever-sample distances.

# 2 EXPERIMENTS WITH A STACK PIEZO

In this chapter, the equations required to analyze a stack piezoelectric transducer with known boundary conditions are presented. Closed form expressions for the impedance and the mechanical frequency response are derived under certain simplifying assumptions. The relation between the impedance curve and the mechanical frequency response is explained and corroborated with experiments.

## 2.1 The Piezoelectric Effect

Piezoelectric effect was first observed by Jacques and Pierre Curie when they first discovered that pressure applied to a quartz crystal creates an electrical charge. Later they also verified that an electrical field applied to the crystal would lead to a deformation of the material. This effect is referred to as the inverse piezo effect. After the discovery in 1880 it took several decades to utilize the piezoelectric effect. The first commercial applications were ultrasonic detectors developed during World War I. Today piezoelectric effect is encountered in daily life. For example, in small butane cigarette gas lighters, a lever applies pressure to a piezoelectric crystal creating an electric field strong enough to produce a spark to ignite the gas. Furthermore alarm clocks often use a piezoelectric element. When AC voltage is applied, the piezoelectric material moves at the source frequency and the resulting sound is loud enough to wake even the strongest sleeper. A very important use of piezos is in the area of nanopositioning. A piezoelectric actuator made of lead zirconium titanate(PZT) has been used in the Atomic Force Microscope

for positioning the sample in order to maintain a constant amplitude (in the tapping mode) or deflection (in the contact mode) in closed loop. Theoretically these actuators provide near zero resolution because they derive their motion through solid state effects and there are no moving parts.

## 2.2 Governing Equations

In this section, a lossless piezoelectric actuator is analyzed by means of constitutive and force balance relations and closed form expressions for the longitudinal displacement and the impedance are derived. In the following equations, the variables are defined as below. Direction 3 is the direction of applied field in all variables. A very good treatment of piezoelectricity is given in [4].

1. $\rho$ – material density of the piezo (in $kg/m^3$)
2. $x_3$ – position in the axial direction. The clamped end is taken to be at position 0
3. L – the axial length of the piezo (in $m$)
4. $u_3(x_3, t)$ – displacement in direction 3 (in $m$)
5. $S_3(x_3, t)$ – axial stress in direction 3 (in $N/m^2$)
6. $\xi_3(x_3, t)$ – strain in direction 3 (no dimensions)
7. $s_{33}^E$ – compliance measured at constant electric field (in $m^2/N$)
8. $d_{33}$ – longitudinal piezoelectric constant (in $m/V$). Here the first subscript refers to the direction of applied electric field and the second subscript refers to the direction of displacement in consideration.
9. $\epsilon_{33}^S$ – dielectric permittivity measured under constant stress (in $C^2/Nm^2$)

10. $E_3(x_3, t)$ – electric field within the piezo (in $V/m$)

11. $D_3(x_3, t)$ – electric displacement vector (in $C/m^2$).

12. $A$ – cross-sectional area of the piezo

Dielectrics are materials which can be polarized upon the application of electric field. The charges within them are attached to specific atoms or molecules. They are however on a "tight leash" and hence can only move a bit within the atom. Hence they are also known as bound charges. In the case of a dielectric with neutral atoms or (non-polar molecules), an applied electric field induces a tiny dipole moment in each atom(or molecule as the case may be), pointing in the field direction. If the dielectric is made up of polar molecules, each permanent dipole will experience a torque again trying to align the dipole in the field direction. Both mechanisms lead to the polarization of the dielectric. The physical quantity describing this effect is called the **Polarization** denoted by $P$ which is by definition the dipole moment induced due to the applied electric field per unit volume of the dielectric.

The modified Gauss's law for dielectrics is given by:

$$\nabla . D = \rho_f \tag{2.1}$$

where $D$ is the dielectric displacement vector which is defined as:

$$D = \epsilon_0 E + P \tag{2.2}$$

where $\epsilon_0$ is the permittivity of free space. A very good treatment on this subject is given in [5].

The following is the force balance equation for an arbitrary longitudinal element of the piezoelectric actuator .

$$\rho \frac{\partial^2 u_3(x_3, t)}{\partial t^2} = \frac{\partial S_3(x_3, t)}{\partial x_3} \tag{2.3}$$

In Equation 2.3 $u_3(x_3,t)$ is the position in direction-3, $S_3(x_3,t)$ is the stress in direction-3 and $t$ is the time in seconds.

The constitutive equations of the stack actuator relating the mechanical strain and the electric field are:

$$\xi_3(x_3,t) = s_{33}^E S_3(x_3,t) + d_{33}E_3(x_3,t) \tag{2.4}$$

$$D_3(x_3,t) = \epsilon_{33}^S E_3(x_3,t) + \frac{d_{33}\xi_3(x_3,t)}{s_{33}^E}. \tag{2.5}$$

In Equations 2.4 and 2.5, $D_3(x_3,t)$ is the dielectric displacement vector, $\xi_3(x_3,t)$ is the strain in direction-3, $s_{33}^E$ is the compliance under constant electric field in direction-3, $\epsilon_{33}^S$ is the dielectric permittivity for electric field in direction-3 and strain in direction-3 under constant stress, $E_3(x_3,t)$ is the electric field in direction-3 and $d_{33}$ is the piezoelectric constant with the subscripts explained as before. Also the constitutive relations are under the assumption that the piezo is thin in the other two width and and thickness directions and there is very little coupling between the three vibration modes.

## 2.3 Electrical and Mechanical Conditions

The electrical condition is given by Gauss's law for dielectrics. The assumption made here is that the piezo material is a pure insulator.

$$\frac{\partial D_3(x_3,t)}{\partial x_3} = 0 \tag{2.6}$$

Equation 2.6 is obtained by using Equation 2.1 and the assumption that the piezoelectric material is a pure insulator, which means that $\rho_f = 0$. The mechanical boundary condition is governed by the way in which the piezo is clamped. If one end of the piezo is clamped, then the mechanical boundary condition is given by the following equations.

$$u_3(0,t) = 0 \tag{2.7}$$

$$S_3(L,t) = 0 \tag{2.8}$$

In Equation 2.8, $L$ represents the length of the stack actuator.

If both the ends of the stack piezo are free then the mechanical boundary conditions are given by the following equations.

$$S_3(0,t) = 0 \tag{2.9}$$

$$S_3(L,t) = 0 \tag{2.10}$$

The electrical condition however remains the same irrespective of either mechanical conditions.

## 2.4 Solution of the PDE

Equation 2.3 can be simplified. First using Equation 2.6 in Equation 2.5 we get

$$\frac{\partial D_3(x_3,t)}{\partial x_3} = \epsilon_{33}^S \frac{\partial E_3(x_3,t)}{\partial x_3} + \frac{d_{33}}{s_{33}^E} \frac{\partial \xi_3(x_3,t)}{\partial x_3} = 0 \tag{2.11}$$

$$\Rightarrow \frac{\partial E_3(x_3,t)}{\partial x_3} = -\frac{d_{33}}{s_{33}^E \epsilon_{33}^S} \frac{\partial \xi_3(x_3,t)}{\partial x_3}. \tag{2.12}$$

Also the displacement and strain are related by Equation 2.26. Hence using Equation 2.26 in Equation 2.12, we get

$$\frac{\partial E_3(x_3,t)}{\partial x_3} = -\frac{d_{33}}{s_{33}^E \epsilon_{33}^S} \frac{\partial^2 u_3(x_3,t)}{\partial x_3^2}. \tag{2.13}$$

Differentiating Equation 2.4 with respect to $x_3$ and using Equation 2.13 and rearranging, we get

$$\frac{\partial S_3(x_3,t)}{\partial x_3} = \frac{1}{s_{33}^E} \frac{\partial^2 u_3(x_3,t)}{\partial x_3^2} + \frac{1}{s_{33}^E} \frac{d_{33}^2}{s_{33}^E \epsilon_{33}^S} \frac{\partial^2 u_3(x_3,t)}{\partial x_3^2} \tag{2.14}$$

$$\frac{\partial S_3(x_3,t)}{\partial x_3} = \frac{1}{s_{33}^D} \frac{\partial^2 u_3(x_3,t)}{\partial x_3^2} \tag{2.15}$$

where

$$s_{33}^D = \frac{s_{33}^E}{1 + k_{33}^2} \tag{2.16}$$

and

$$k_{33}^2 = \frac{d_{33}^2}{s_{33}^E \epsilon_{33}^S}. \tag{2.17}$$

Hence Equation 2.3 now becomes

$$\frac{\partial^2 u_3(x_3,t)}{\partial t^2} = \frac{1}{\rho s_{33}^D} \frac{\partial^2 u_3(x_3,t)}{\partial x_3^2}. \tag{2.18}$$

Hence the partial differential equation that needs to be solved is

$$v'^2 \frac{\partial^2 u_3(x_3,t)}{\partial x_3^2} = \frac{\partial^2 u_3}{\partial t^2} \tag{2.19}$$

where

$$v' = \sqrt{\frac{1}{s_{33}^D \rho}} \tag{2.20}$$

with boundary conditions

$$u_3(0,t) = 0 \tag{2.21}$$

$$b_1 \frac{\partial u_3(L,t)}{\partial x_3} + b_2 u_3(L,t) = V(L,t) \tag{2.22}$$

and with initial conditions (assuming flat initial mode shapes) given by

$$u_3(x_3,0) = 0 \tag{2.23}$$

$$\frac{\partial u_3}{\partial x_3}(x_3,0) = 0 \tag{2.24}$$

where the constants $v'$,$b_1$ and $b_2$ are known.

Rearranging Equation 2.4 we get

$$S_3(L,t) = 0 \Leftrightarrow \frac{1}{s_{33}^E}[\xi_3(x_3,t) - d_{33}E_3(x_3,t)]|_{x_3=L} = 0. \tag{2.25}$$

Also we have the following relationship between displacement and strain

$$\xi_3(x_3,t) = \frac{\partial u_3(x_3,t)}{\partial x_3}. \tag{2.26}$$

Using Equation 2.26 in Equation 2.25 and rearranging terms we have

$$S_3(L,t) = 0 \Leftrightarrow \frac{\partial u_3(L,t)}{\partial x_3} = d_{33}E_3(L,t). \tag{2.27}$$

Using Equation 2.26 in Equation 2.5 and rearranging terms, we have

$$D_3(t) = \epsilon_{33}^S E_3(x_3,t) + \frac{d_{33}}{s_{33}^E}\frac{\partial u_3(x_3,t)}{\partial x_3} \tag{2.28}$$

$$\Rightarrow \int_0^L D_3(t)dx_3 = \epsilon_{33}^S \int_0^L E_3(x_3,t)dx_3 + \frac{d_{33}}{s_{33}^E}\int_0^L \frac{\partial u_3(x_3,t)}{\partial x_3}dx_3 \tag{2.29}$$

$$= \epsilon_{33}^S[V(L,t) - V(0,t)] + \frac{d_{33}}{s_{33}^E}[u_3(L,t) - u_3(0,t)]. \tag{2.30}$$

Using Equation 2.6 in the left hand side of Equation 2.29 we get

$$\Rightarrow D_3(t) = \frac{\epsilon_{33}^S}{L}V(L,t) + \frac{d_{33}}{s_{33}^E L}u_3(L,t). \tag{2.31}$$

Also from Equation 2.28 we have

$$E_{33}(x_3,t) = \frac{D_3(t)}{\epsilon_{33}^s} - \frac{d_{33}}{s_{33}^E\epsilon_{33}^S}\frac{\partial u_3(x_3,t)}{\partial x_3}. \tag{2.32}$$

From Equation 2.31 we have

$$E_{33}(L,t) = \frac{1}{\epsilon_{33}^S}[\frac{\epsilon_{33}^S}{L} + \frac{d_{33}}{s_{33}^E L}u_3(L,t)] - \frac{d_{33}}{s_{33}^E\epsilon_{33}^S}\frac{\partial u_3}{\partial x_3}(L,t). \tag{2.33}$$

Substituting Equation 2.33 in Equation 2.27 we have

$$S_3(L,t) = 0 \Leftrightarrow b_1\frac{\partial u_3(L,t)}{\partial x_3} + b_2 u_3(L,t) = V(L,t) \tag{2.34}$$

where

$$b_1 = \frac{L}{d_{33}}[1 + \frac{d_{33}^2}{s_{33}^E\epsilon_{33}^s}] \tag{2.35}$$

$$b_2 = -\frac{d_{33}}{s_{33}^E\epsilon_{33}^S}. \tag{2.36}$$

Next variables $z_1(t)$ and $z_2(t)$ are defined as follows

$$z_1(t) = u_3(x_3,t), z_1(t)\varepsilon L_2[0,L] \tag{2.37}$$

$$z_2(t) = \frac{du_3(x_3,t)}{dx_3} = \frac{dz_1(t)}{dt}, z_2(t)\varepsilon L_2[0,L]. \tag{2.38}$$

Taking Laplace transform of Equation 2.19 with respect to $t$ and using Equations 2.37 and 2.38, we have

$$v'^2 \frac{d^2 \hat{z}_1(s)}{dx_3^2} = s^2 \hat{z}_1(s) \tag{2.39}$$

$$v'^2 \frac{d\hat{z}_2(s)}{dx_3} = s^2 \hat{z}_1(s). \tag{2.40}$$

Therefore we have

$$\frac{d}{dx_3} \begin{bmatrix} \hat{z}_1 \\ \hat{z}_2 \end{bmatrix} = \begin{bmatrix} 0 & 1 \\ s^2 & 0 \end{bmatrix} \begin{bmatrix} \hat{z}_1 \\ \hat{z}_2. \end{bmatrix} \tag{2.41}$$

Also taking Laplace transform of Equations 2.21 and 2.22 with respect to $t$ we have

$$z_1(0, s) = 0 \tag{2.42}$$

$$b_1 z_2(L, s) + b_2 z_1(L, s) = V(L, s) \tag{2.43}$$

Next let us define a state variable $z$ as

$$z = \begin{bmatrix} z_1 \\ z_2. \end{bmatrix} \tag{2.44}$$

Equation 2.41 is an ordinary differential equation in $x_3$ and its solution is given by

$$z(x_3, s) = \begin{bmatrix} \cosh(\frac{sx_3}{v'}) & \frac{v'}{s}\sinh(\frac{sx_3}{v'}) \\ \frac{s}{v'}\sinh(\frac{sx_3}{v'}) & \cosh(\frac{sx_3}{v'}) \end{bmatrix} \begin{bmatrix} \hat{z}_1(0, s) \\ \hat{z}_2(0, s) \end{bmatrix} \tag{2.45}$$

$$\Rightarrow z(x_3, s) = \begin{bmatrix} \frac{v'}{s}\sinh(\frac{sx_3}{v'})\hat{z}_2(0, s) \\ \cosh(\frac{sx_3}{v'})\hat{z}_2(0, s) \end{bmatrix} \tag{2.46}$$

Using Equation 2.46 in Equation 2.43 we get

$$b_1 \cosh(\frac{sx_3}{v'})\hat{z}_2(0, s) + b_2 \frac{v'}{s}\sinh(\frac{sx_3}{v'})\hat{z}_2(0, s) = V(L, s) \tag{2.47}$$

$$\Rightarrow \hat{z}_2(0, s) = \frac{V(L, s)}{b_1 \cosh(\frac{sx_3}{v'}) + \frac{b_2 v'}{s}\sinh(\frac{sx_3}{v'})} \tag{2.48}$$

$$\Rightarrow z_1(x_3,s) = u_3(x_3,s) = V(L,s)\frac{v'}{s}\left(\frac{\sinh(\frac{sx_3}{v'})}{b_1\cosh(\frac{sx_3}{v'}) + \frac{b_2v'}{s}\sinh(\frac{sx_3}{v'})}\right). \tag{2.49}$$

Substituting Equation 2.48 back in Equation 2.45 and defining $z_1(L,s) = u_3(L,s)$ as the output and $V(L,s)$ as the input we get the following transfer function

$$\frac{u_3(L,s)}{V(L,s)} = \frac{v'}{s}\left(\frac{\sinh(\frac{sL}{v'})}{b_1\cosh(\frac{sL}{v'}) + \frac{b_2v'}{s}\sinh(\frac{sL}{v'})}\right) \tag{2.50}$$

$$M(\omega) = \frac{u_3(L,\omega)}{V(\omega)} = \frac{d_{33}\frac{\tan kL}{kL}}{(1+k_{33}^2)(1-k_t^2\frac{\tan kL}{kL})} \tag{2.51}$$

where $k_t$ is defined as

$$k_t^2 = \frac{k_{33}^2}{1+k_{33}^2}. \tag{2.52}$$

The next objective is to derive an expression for the impedance of the stack piezo. The current is given by:

$$I(s) = s\int_A D_3(x_3,s)dx_2dx_1 = sD_3(s)A \tag{2.53}$$

where $A$ is the cross sectional area of the piezo which is a constant. Also $D_3(x_3,s)$ can be taken out of the integral in Equation 2.53.

Taking Laplace transform of Equation 2.31 and using Equation 2.50, we get

$$D_3(s) = \frac{\epsilon_{33}^S V(L,s)}{L}\left[1 + \frac{k_{33}^2v'}{sL(1+k_{33}^2)\coth(\frac{v'L}{s}) - \frac{k_{33}^2v'}{s}}\right]V(L,s). \tag{2.54}$$

Eliminating $D_3(s)$ from Equations 2.53 and 2.54, we get the impedance of the piezo as

$$Z(s) = \frac{V(s)}{I(s)} = \frac{L}{\epsilon_{33}^S As}\frac{\frac{sL}{v'}\frac{\coth(\frac{v'L}{s})}{k_t^2} - 1}{\frac{sL}{v'}\frac{\coth(\frac{v'L}{s})}{k_t^2}}. \tag{2.55}$$

Substituting $s = j\omega$ in Equation 2.55 we get

$$Z(\omega) = \frac{V(\omega)}{I(\omega)} = L\frac{1 - \frac{k_{33}^2}{1+k_{33}^2}\frac{\tan kL}{kL}}{j\omega\epsilon_{33}^S A}. \tag{2.56}$$

This impedance can be rewritten as admittance also with two branches in parallel.

$$Y = Y_o + Y_p \tag{2.57}$$

$$Y_o = j\omega C_o \tag{2.58}$$

$$C_o = \frac{\epsilon_{33}^S A}{L} \tag{2.59}$$

$$k_t^2 = \frac{k_{33}^2}{1 + k_{33}^2} \tag{2.60}$$

$$b = kL \tag{2.61}$$

$$Y_p = \frac{j\omega C_o}{-1 + \frac{1}{k_t^2 \frac{\tan b}{b}}}. \tag{2.62}$$

Equations 2.57 through 2.62 indicate that the impedance of the stack can be viewed as a pure capacitor $C_0$ at low frequencies and a group of parallel elements which contribute to the resonance/antiresonance phenomenon at high frequencies.

## 2.5 Analysis

In this section the equations for the mechanical response (2.51) and impedance (2.56) are analyzed to obtain resonant/antiresonant frequencies. In general the impedance curve of a piezoelectric transducer has infinite resonant/anti-resonant frequency pairs. This is shown by analyzing Equation 2.56. Antiresonance occurs when the impedance tends to 0. Mathematically this happens when

$$1 - \frac{k_t^2 \tan b}{b} = 0 \tag{2.63}$$

Resonance occurs when the impedance tends to $\infty$. This happens when

$$\frac{\tan b}{b} = \infty. \tag{2.64}$$

It is to be noted that resonance occurs at odd multiples of the first resonance.

Interestingly the mechanical transfer function of the tip given by Equation 2.51 exhibits a resonance for the same condition 2.64 as for electrical resonance. Equations 2.64

and 2.63 have infinite number of solutions and hence there are infinite resonant/anti-resonant frequencies in the impedance plot and for every electrical antiresonance, a mechanical resonance should be present. Such relations are very important for piezoelectric actuators because the the mechanical frequency response is usually difficult to obtain experimentally because of non-availability of sensors which can detect displacements at high frequencies. However, the impedance curve can be very easily obtained by means of a control systems analyzer and the above relationships enable us to predict the mechanical frequency response of the piezo after obtaining the impedance curve experimentally.

Also from 2.51 and 2.56 we get

$$M(\omega) = \frac{d_{33} \tan kL}{j\omega k(1 + k_{33}^2)\epsilon_{33}^S AZ(\omega)} \tag{2.65}$$

which is a direct relationship between the electrical impedance and the mechanical response.

## 2.6 Experiments

In this section, experimental evidence is provided to corroborate the theoretical derivations presented in the previous section. The derivations were presented for a piezoelectric actuator with boundary conditions given by Equations 2.7 and 2.8, which mean that the stack is clamped at one end. Experimentally this condition was obtained by glueing the free end of a stack actuator (AE505D16 from Tokin America) to a metal puck using 2-minute epoxy. First, the impedance plot was obtained using the HP-3563A Control Systems analyzer. A 50$\Omega$ resistor was soldered to one end negative electrode of the stack to indirectly measure the current as the voltage across the same. Figure 2.1 is the impedance curve obtained experimentally.

At low frequencies, the impedance of the piezo looks like a pure capacitor as predicted

by Equation 2.58. At high frequencies two resonant/anti-resonant modes are seen. The observations are tabulated below.

$$f_{a_1} = 28.022KHz \tag{2.66}$$

$$f_{r_1} = 31.441KHz \tag{2.67}$$

$$f_{a_2} = 83.656KHz \tag{2.68}$$

$$f_{r_2} = 90.678KHz. \tag{2.69}$$

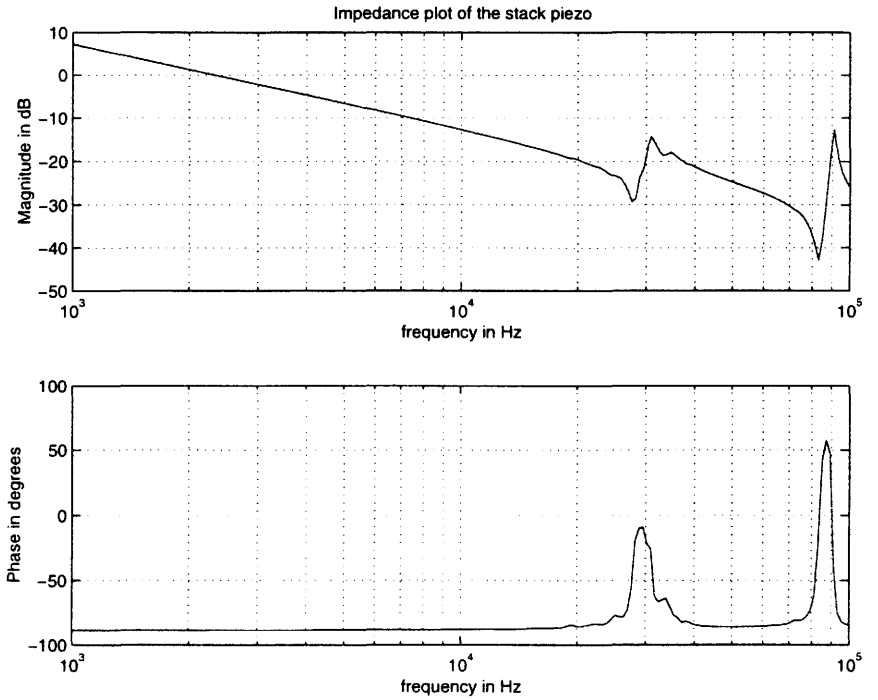


Figure 2.1 The impedance curve of the stack piezo showing the unique resonant/antiresonant behaviour in the phase response and a phase jump in the phase response

where the subscripts $r$ and $a$ refer to resonance and anti-resonance respectively and subscripts 1 and 2 denote the first and second instances of the same.

According to the theory presented in the previous sections, it is expected that the mechanical frequency response should have two resonant frequencies at $31.441KHz$ and $90.678KHz$ repectively. Also

$$f_{r_2} = 3f_{r_1} \tag{2.70}$$

which is in accordance with the theory presented above.

In order to obtain the mechanical response the Atomic Force Microscope(AFM) was utilized. A contact mode cantilever was mounted on the free face of the stack piezo. Manual screws were adjusted to ensure that the cantilever was in contact with the stack. In this condition, the movement of the piezo was directly measured as the photodiode output. A frequency sweep from 1Hz to 100KHz was performed and the response obtained for various DC offsets of the piezo is as shown in Figure 2.2.

The mechanical response shows peaks at $f_{m_{r_1}} = 30.309Khz$ and $f_{m_{r_2}} = 89.993Khz$ which are pretty close to $f_{r_1}$ and $f_{r_2}$. The uncertainty at DC is due to hysteresis which is a static non-linearity. There are other peaks also seen at frequencies other than the predicted ones. These might be due to the coupling between the longitudinal and transverse mode which has been neglected in the derivation presented in this chapter.

## 2.7 Conclusions

In this chapter, a theoretical relationship between the mechanical frequency response and the impedance of the stack was derived. Experimental evidence was shown to prove the existence of mechanical resonances at the electrical resonant frequencies. Linear constitutive relations were assumed to exist relating the electric displacement, electric field,axial stress and strain within the piezoelectric actuator. The AFM was used to get mechanical response plots by using the contact mode cantilever to get detect the displacement of the free end of the piezo. A favorable match was seen in the resonant

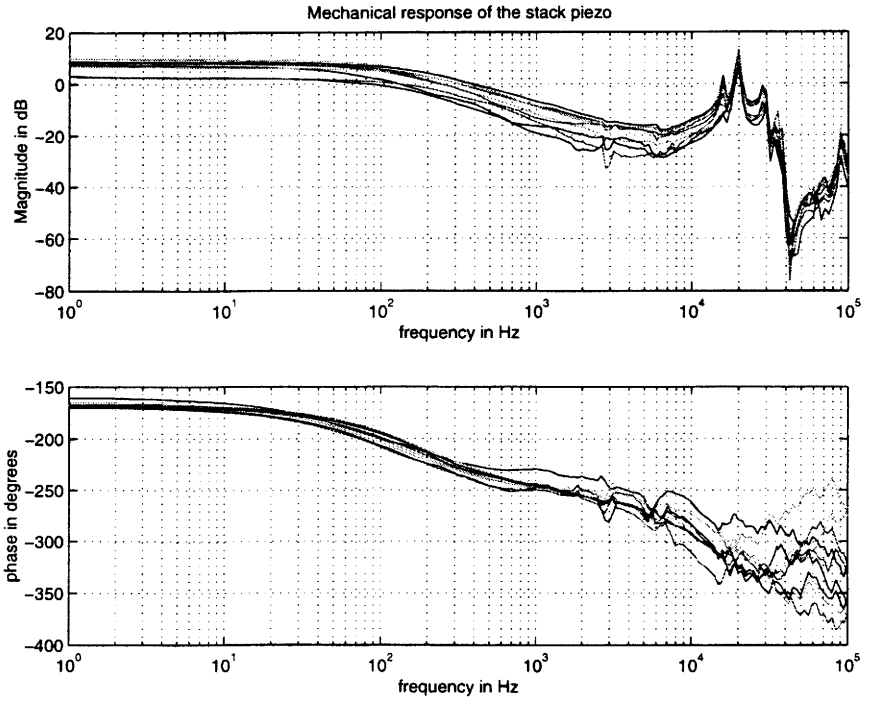


Figure 2.2 The mechanical response shows uncertainty at DC frequency. The curves for different DC offsets merge at high frequencies

frequencies as predicted by the equations. Furthermore, a direct relationship between the impedance and mechanical frequency response was derived (Equation 2.65) which can be used in later work to predict the mechanical frequency response by just making electrical measurements and with the knowledge of material constants. Future work involves using the mechanical transfer function (Equation 2.51) to evaluate the limitations of performance of the stack piezo and also using it to build controllers to achieve performance objectives like tracking and disturbance rejection.

# 3 IDENTIFICATION OF MICRO-CANTILEVERS IN ATOMIC FORCE MICROSCOPES

In this chapter, a method of estimating the mass and stiffness of the micro-cantilever used as a probe in the Atomic Force Microscope is presented. Noise has always been treated as an unwanted signal by engineers. Chapter 1 has indicated that noise can be used to estimate optimal cantilever-sample separations to improve the sensitivity of the micro-cantilever while scanning the surface of the sample. In this chapter, thermal noise characterization of micro-cantilevers used as a probe in scanning probe microscopes is discussed. Experimentally obtained thermal noise response is used to obtain the spring constant of the micro-cantilever. Also this provides a method to obtain the mass of the cantilever, as the resonant frequency is a function of both the spring constant and the mass. The theory and experimental evidence of the thermal noise characterization is discussed with greater detail in [7].

## 3.1 Thermal Noise Characterization of the Micro-cantilever

One of the main components in the Atomic Force Microscope is the micro-cantilever which is used to probe the sample surface. The stiffness of the micro-cantilever should be such that it should deflect even for the piconewton force levels that it experiences when it is at extremely close distances to the sample surface. Hence a method for obtaining the stiffness of the cantilever is of utmost importance,as this constant would be used to estimate the force gradient that the cantilever experiences when it scans the surface

of different samples. The cantilever is assumed to be in thermal equilibrium with the environment, which means that there is no exchange of energy between the cantilever and the surroundings. Then the law of equipartition of energy says that the total energy of the cantilever is equally divided as kinetic and potential energies on an average.

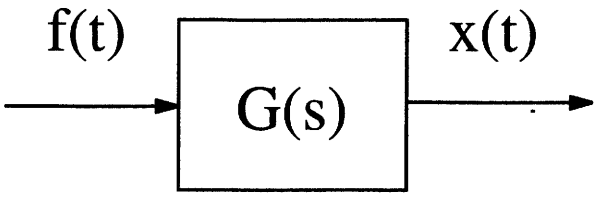


Figure 3.1 The micro-cantilever subjected to thermal noise $f(t)$

$$< TE >=< PE > + < KE > \tag{3.1}$$

$$< PE >=< KE >= \frac{1}{2} < TE > \tag{3.2}$$

where $< TE >$ is the expected value of total energy of the cantilever, and $< PE >$ and $< KE >$ are the expected values of the potential and kinetic energies of the cantilever. From quantum mechanics, the total energy of the cantilever (thought of as a simple harmonic oscillator) is given by

$$< TE >= \frac{\hbar\omega_0}{\exp \frac{\hbar\omega_0}{k_b T} - 1} \tag{3.3}$$

where $\hbar = \frac{h}{2\pi}$, $\omega_0 = \sqrt{\frac{k}{m}}$ where $k$ and $m$ were defined previously, $k_b$ is the Boltzmann's constant and $T$ is the ambient temperature in Kelvin. If we assume that $\hbar\omega_0 << k_b T$, then Equation 3.3 becomes

$$< TE >= k_b T \tag{3.4}$$

Applying the law of equipartition of energy we have

$$< PE >= \frac{1}{2} k_b T \tag{3.5}$$

All expressions above were derived from quantum mechanical laws that are universally applicable to all systems. However, the cantilever can be approximated classically with a second order dynamical equation given by Equation 3.6

$$m\ddot{q} + c\dot{q} + kq = f(t) \tag{3.6}$$

where $m$ is the mass of the cantilever,$c$ is the damping factor cantilever,$k$ is the stiffness of the cantilever, $q(t)$ is the displacement of the cantilever from its equilibrium position and $f(t)$ is the thermal noise input. In [7], a detailed discussion of this approximation is presented where the higher modes of the cantilever are neglected. Under such conditions the cantilever can be thought of as a linear system described by Equation 3.6 being subjected to thermal noise forcing $f(t)$, which can be modeled as a filtered white noise process. Hence classical laws can also be applied to arrive at an expression for the average potential energy of the cantilever which is given by

$$< PE >= \frac{1}{2}k < q^2(t) > \tag{3.7}$$

where $< q^2(t) >$ is the variance of the displacement of the cantilever from its equilibrium position. Since both classical and quantum mechanical laws are applicable to the cantilever, Equation 3.5 and Equation 3.7 are the same. Hence

$$\frac{1}{2}k_bT = \frac{1}{2}k < q^2(t) > \tag{3.8}$$

The variance of the displacement $< q^2(t) >$ can be obtained from the power spectral density of the displacement $S_{qq}$ using the following equations.

$$R_{qq}(\tau) =< (q(t)q(t+\tau)) > \tag{3.9}$$

$$\Rightarrow R_{qq}(0) =< q^2(t) > \tag{3.10}$$

$$R_{qq}(\tau) = \int_{-\infty}^{\infty} S_{qq}(f)e^{j2f\pi}df \tag{3.11}$$

$$< q^2(t) >= R_{qq}(0) = \int_{-\infty}^{\infty} S_{qq}(f)df \tag{3.12}$$

where $R_{qq}(\tau)$ is the autocorrelation function of the displacement of the cantilever from its mean position.

Using Equation 3.12 in Equation 3.8 we get

$$k = \frac{k_b T}{\int_{-\infty}^{\infty} S_{qq}(f) df} \tag{3.13}$$

Hence using Equation 3.13 we can obtain the spring constant of the cantilever.

## 3.2 Estimation of the Mass of the Cantilever

The resonant frequency of the cantilever $\omega_0$ is related to the mass $m$ and the stiffness $k$ by

$$\omega_0 = \sqrt{\frac{k}{m}} \tag{3.14}$$

From Section 3.1, the stiffness is obtained and can be used in Equation 3.14 to obtain the mass as follows

$$m = \frac{k}{\omega_0^2} \tag{3.15}$$

## 3.3 Experiments

In order to obtain the stiffness parameter of the cantilever two experiments need to be performed. The first experiment is to obtain the power spectral density of the thermal noise response of the cantilever. The Control Systems Analyzer(CSA) was used for this purpose. This photodiode output was obtained using the IN0 pin of the Signal Access Module described in Chapter . This was fed into the CSA as shown in Figure 3.2. An MFM(magnetic force microscope) cantilever was chosen for experimental purposes. The length of the cantilever was around 250 microns and the resonant frequency was seen to be 80.5kHz. The experimentally observed PSD curve is as seen below The PSD was averaged long enough so that the first mode of the cantilever is seen without any noise riding over it. It is evident from Figure 3.2 that the area under the peak of the

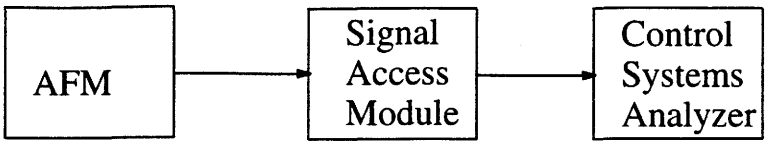


Figure 3.2 Interconnection of the components involved to obtain the PSD of the cantilever's thermal noise response

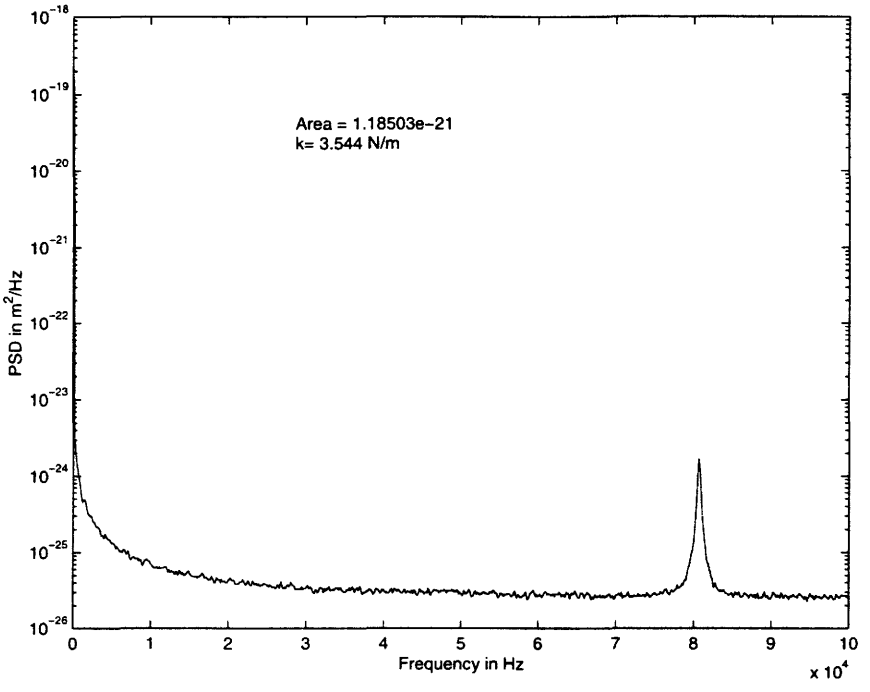


Figure 3.3 Experimentally observed PSD curve of the MFM cantilever

first mode contributes the most to the total area (The y-axis is in log scale). Also the PSD curve is one sided in frequency domain. Hence Equation 3.13 can be modified as

$$k = \frac{k_b T}{\int_{f_1}^{f_2} S_{qq}(f) df} \tag{3.16}$$

where $f_1$ and $f_2$ are the frequencies between which the peak of the first mode lies.

The second experiment was to obtain the force curve of the cantilever and calibrate the sensitivity of the photodiode as explained in Chapter 3.3. The approach and retract parts of the repulsive region were not parallel, hence an average of the slopes of the two

repulsive region lines was taken as the sensitivity of the photodiode. The result is as shown in Figure

The sensitivity information was used to convert the photodiode voltage into displacement units. The estimated spring constant was found to be 3.544N/m. The mass of the cantilever was found using Equation 3.15 to be 1.385e-11kg. For calculation purposes $k_bT$ was taken to be 4e-21J at room temperature(300K). 3.4. The inherent noise level

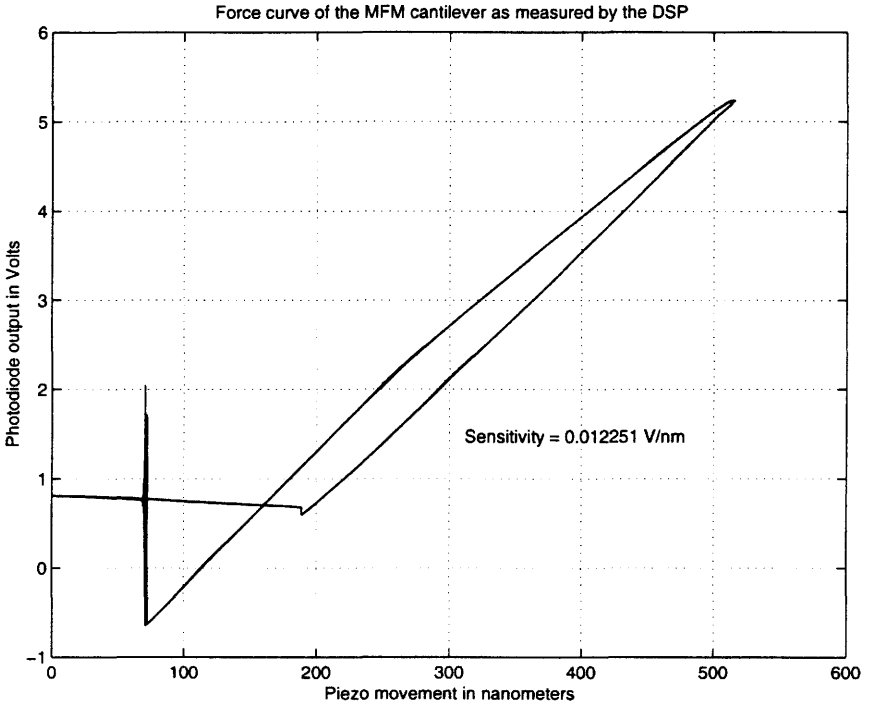


Figure 3.4 Experimentally observed force curve of the MFM cantilever

in the flat part of the PSD curve in Figure 3.3 is found to be higher in air as compared to that in water. Hence the same experiment when performed in water will give a better estimate of the spring constant. The effect of performing it in water can be thought of as changing the mass $m$ and the damping factor $c$ of the cantilever, however the stiffness $k$ remains unaffected as this is a property of the material that is used in manufacturing the cantilever. Hence the dynamical equation 3.6 can be assumed to be the same for the cantilever in water, giving the same value of $k$ for the cantilever in air and in water.

## 3.4 Conclusions

In this chapter a method has been provided to estimate the spring constant of the first mode of the cantilever using the thermal noise response of the cantilever. This method utilizes the fact the micro-cantilever is a device which can respond to thermal noise and the potential energy of the cantilever when in equilibrium with the surrounding can be derived both classically and quantum mechanically, and these two expressions can be equated to obtain the spring constant of the cantilever. Also the method helps in estimating the mass of the cantilever neglecting the higher modes.

# BIBLIOGRAPHY

[1] Bulsara A.R. and Gammaitoni L. Tuning in to noise. *Nature*, 373:39–45, 1996.

[2] M. Ashhab, M. V. Salapaka, M. Dahleh, and I. Mezic. Dynamical analysis and control of micro-cantilevers. *Automatica*, 35:1663–1670, 1999.

[3] Mezic M. Salapaka M. V. Basso M., Dahleh M. Stochastic resonance in afm's. In *Proceedings of the American Control Conference*, June 1999.

[4] Takuro Ikeda. *Fundamentals of Piezoelectricity.* Oxford University Press, Tokyo, 1990.

[5] Griffiths J.David. *Introduction to electrodynamics.* Englewood Cliffs, New Jersey, 1999.

[6] Weisenfield K. McNamara B. Theory of stochastic resonance. *Physical Review A*, 39:4854–4869, 1983.

[7] M. V. Salapaka, H. S. Bergh, J. Lai, A. Majumdar, and E. McFarland. Multimode noise analysis of cantilevers for scanning probe microscopy. *Journal of Applied Physics*, 81(6):2480–2487, 1997.

[8] Chen D. J. Cleveland J. P. Sebastian A., Salapaka M. V. Harmonic analysis based modeling of tapping-mode afm. *Proceedings of the American Control Conference*, 1999.

[9] Gardiner C. W. *Handbook of Stochastic Methods for Physics, Chemistry, and the Natural Sciences.* Springer-Verlag, Berlin, 1983.

[10] K. Wiesenfeld and F. Moss. Stochastic resonance and the benefits of noise: From ice ages to crayfish and squids. *Nature*, 373:33–36, 1995.